Iranian Journal of Numerical Analysis and Optimization
Vol. ??, No. ??, ??, pp ??
https://doi.org/??
https://ijnao.um.ac.ir/

Research Article

Understanding the impact of vaccination on Omicron variants

G.P. Sahu, A.S. Thakur*, C.S. Sikarwar and H. Singh

Abstract

The COVID-19 pandemic, caused by the SARS-CoV-2 virus, has led to the emergence of multiple variants, including Alpha, Beta, Gamma, Delta, and Omicron, each exhibiting distinct transmissibility and severity profiles. In this context, a new deterministic mathematical model has been developed as an extension of Thakur and Sahu [51], designed to capture the dynamics of COVID-19 transmission while incorporating the effects of both the first and second doses of vaccination. The model is examined using the theory of dynamical systems. The basic reproduction number is derived, and both the local stability of the disease-free and endemic

*Corresponding author

Received ??? ; revised ??? ; accepted ???

Govind Prasad Sahu
Center for Basic Sciences, Pt. Ravishankar Shukla University, Raipur, Chhattisgarh. e-mail: govind3012@gmail.com

Amit Singh Thakur
School of Studies in Mathematics, Pt. Ravishankar Shukla University, Raipur, Chhattisgarh. e-mail: amitsinghprsu@gmail.com

Chhatrpal Singh Sikarwar
Department of Mathematics, Govt Kachna Dhurwa College Chhura, Chhattisgarh. e-mail: chhatrapal84@gmail.com

Harkaran Singh
College of Trades, Technology, and Hospitality, Victoria University, Footscray, Victoria 3011, Australia. e-mail: harkaran1978@gmail.com

How to cite this article
Sahu, G.P., Thakur, A.S., Sikarwar, C.S. and Singh, H., Understanding the impact of vaccination on Omicron variants. *Iran. J. Numer. Anal. Optim.*, ??; ??(??): ??-??. ??

equilibria, as well as the global stability of the disease-free equilibrium, are established. The model is calibrated using data from India's third wave of the COVID-19 pandemic. Sensitivity analysis, employing partial rank correlation coefficients and normalized forward sensitivity indices, identifies vaccination rates as key parameters driving disease dynamics. Findings reveal that the Omicron variant has the potential to cause large-scale outbreaks even with ongoing vaccination campaigns. The study emphasizes the need for sustained high vaccination coverage and the continued implementation of nonpharmaceutical interventions to control the pandemic effectively. Furthermore, the model is extended to an optimal control framework, concluding that dynamically adjusting five targeted control measures offers the most effective strategy for reducing infections while minimizing associated costs.

AMS subject classifications (2020): Primary 92D30; Secondary 92C60.

Keywords: COVID-19; Environmental transmission; Vaccination; Optimal control; Omicron.

1 Introduction

COVID-19, caused by the SARS-CoV-2 virus, has emerged as one of the most significant public health crises of the 21st century, profoundly impacting global health, economies, and societies. Since its emergence in late 2019, the virus has spread rapidly worldwide, exposing vulnerabilities in healthcare infrastructure and pandemic preparedness [57]. During the early stages of the pandemic, when biomedical interventions were not yet widely available, nonpharmaceutical measures—such as spreading information through television, radio, social media, and the Internet—played a crucial role in reducing disease transmission [50, 49]. Media coverage played a critical role in influencing public behaviour, encouraging preventive actions such as mask-wearing, social distancing, quarantine, and isolation [35]. While these measures reduced transmission risk, they were insufficient on their own to contain the pandemic [15].

Vaccination quickly became central to mitigating the impact of COVID-19, as vaccines prepared the immune system to fight infection [45, 29]. By early 2021, the distribution of vaccines had significantly improved the global pandemic outlook. In India, the vaccination campaign began on January 16, 2021, and by December 31, 2021, approximately 89% of the population had received at least one dose [48]. Despite these achievements, SARS-CoV-2 continued to evolve, with variants such as Alpha, Beta, Gamma, Delta, and Omicron emerging [10]. Although vaccines developed against early variants exhibited reduced efficacy against Delta and Omicron, they continued to provide substantial protection against severe disease [23, 47]. The Delta variant

in particular demonstrated increased transmissibility, shorter incubation periods, higher viral loads, and greater disease severity [9].

The Omicron variant, first reported in November 2021 in South Africa [36], rapidly became dominant worldwide. In India, Omicron's prevalence rose dramatically, from 0.35% to over 97% between November 29, 2021, and February 7, 2022 [44]. This surge led to record infection rates in cities such as Mumbai, where daily cases escalated from 191 to over 20,000 by early January 2022 [44]. Omicron exhibited higher transmissibility than previous variants, contributing to widespread infections, particularly among younger, less-vaccinated populations [31, 18].

Mathematical modeling has played a pivotal role in understanding COVID-19 transmission dynamics and guiding public health interventions, especially in India [3, 24, 41, 5, 27, 6, 40]. Researchers have developed various compartmental models to simulate the spread of disease and assess control strategies. For instance, Bagal et al. [3] simulated COVID-19 transmission, Bajiya et al. [5] emphasized the role of face masks and quarantine, and Negi et al. [27] introduced an SEIAHR framework incorporating vaccination and quarantine. Bandekar et al. [6] analyzed India's third wave, highlighting the benefits of mask compliance, screening, and timely treatment. Sahu and Thakur [38] analyzed how media influence, environmental factors, and treatment capacity constraints affect the spread of epidemics in India.

Recent modeling studies have recognized the importance of environmental contamination in transmission [40, 26, 51, 37]. The virus can remain viable on surfaces for days, and infected individuals contribute to environmental contamination through respiratory droplets [14, 54]. Modern epidemic models have evolved beyond classical SEIR frameworks [32], incorporating deaths [42, 43], isolation [34], asymptomatic infection [39], hospitalization [41], and vaccination strategies [27, 22, 46, 11], thus enabling realistic simulation of interventions.

Several studies have specifically assessed vaccination's role in pandemic control, including multi-dose strategies [12, 27, 22, 46, 11, 4, 17, 56]. By the end of 2021, 64% of India's population was fully vaccinated with two doses [48], and two doses of Covishield or Covaxin significantly reduced infection risk according to the Indian Council of Medical Research.

In this work, we develop a mathematical modeling framework to investigate the combined effects of vaccination and environmental transmission on the spread of COVID-19 in India during the Omicron wave. The proposed model incorporates partially and fully vaccinated populations together with environmental viral dynamics [17, 56, 51], enabling a realistic assessment of intervention strategies. Using real epidemiological data and optimal control techniques, the study aims to guide policymakers in designing effective mitigation measures against future SARS-CoV-2 outbreaks [1, 5, 28, 58, 19].

The organization of this work is as follows: Section 2 presents a novel mathematical model that captures the dynamics of COVID-19 transmission. In Section 3, we examine the model's

well-posedness, characterize equilibrium points, analyze stability properties, and derive the control reproduction number along with possible bifurcations. Section 4 focuses on numerical analyses, including parameter estimation from real-world data, sensitivity assessments using normalized and partial rank correlation coefficients (PRCC) methods, and simulations evaluating the influence of dual vaccine doses and environmental factors on disease spread. Section 5 formulates and solves an optimal control problem related to the model. Finally, Section 6 summarizes the main findings and outlines future research directions.

2 Mathematical model

The human population $N(t)$ within a given community is divided into eight compartments, each representing a different stage in the disease dynamics: susceptible individuals $S(t)$, exposed individuals $E(t)$, asymptomatic carriers $I_a(t)$, symptomatic infected individuals $I(t)$, those infected with the Omicron variant $I_0(t)$, individuals who have received the first vaccine dose $V_1(t)$, those who have received the second dose $V_2(t)$, and recovered individuals $R(t)$. Additionally, the environmental concentration of the virus is denoted by $U(t)$. Hence, the total population at any time t is given by

$$N(t) = S(t) + E(t) + I_a(t) + I(t) + I_0(t) + V_1(t) + V_2(t) + R(t).$$

We propose the following assumptions:

- The population is uniformly spread out, with new individuals consistently entering the susceptible group at a fixed rate Λ, while natural deaths occur at a constant rate μ.
- The parameter β represents the transmission rate at which a susceptible individual contracts an infection through valid contact with infected individuals (asymptomatic, symptomatic, and Omicron-infected individuals). Parameters η_1 and η_2 represent the relative infectiousness of individuals with symptomatic and Omicron variant infections, respectively, compared to asymptomatic individuals.
- The latent period of infected individuals is represented by $1/\sigma$. After the latent period, exposed individuals who do not exhibit clinical symptoms join the asymptomatic infected class at a rate of $\sigma\psi$. Individuals who develop clinical symptoms of COVID-19 progress to the symptomatic infected compartment at a rate $\sigma(1-\psi-\phi)$. In contrast, the remaining exposed individuals transition to the Omicron-infected compartment at a rate $\phi\sigma$.

- Individuals at risk of COVID-19 receive a first vaccine dose (Dose I) at rate ν_1, providing partial immunity. However, this immunity wanes over time, and individuals vaccinated with Dose I gradually return to the susceptible class at rate ω_1 [14, 11]. Additionally, protection from Dose I is incomplete, leaving some individuals partially susceptible, with reduced susceptibility quantified by the factor θ [56]. Administration of a second vaccine dose (Dose II) at rate ν_2 leads to optimal protection, substantially lowering the risk of reinfection [4, 17, 21].

- Symptomatic individuals transition to the recovered category at a recovery rate of γ_2, whereas those infected with the Omicron variant recover at a different rate, γ_3. Asymptomatic cases, which do not show visible symptoms, recover on their own and join the recovered group at a rate γ_1. Over time, immunity in recovered individuals wanes, causing a portion of them to revert to the susceptible group at a rate denoted by χ.

- Individuals showing symptoms and those infected with the Omicron variant succumb to the disease at respective rates denoted by δ_1 and δ_2.

- Individuals infected with COVID-19 emit the virus into the environment primarily via respiratory activities such as coughing and sneezing. The environmental contribution rates of asymptomatic, symptomatic, and Omicron-infected individuals are represented by θ_1, θ_2, and θ_3, respectively. Despite this shedding, the virus has a limited environmental lifespan due to factors such as disinfection efforts and natural decay, with its removal from the environment occurring at a rate ϵ.

Based on the above assumptions, the spread of COVID-19 can be modeled using the following system of nonlinear ordinary differential equations:

$$
\begin{cases}
\frac{dS}{dt} &= \Lambda - \frac{\beta(\eta_1 I + I_a + \eta_2 I_0)S}{N} - \beta_1 U S - \nu_1 S + \omega_1 V_1 + \chi R - \mu S, \\
\frac{dE}{dt} &= \frac{\beta(\eta_1 I + I_a + \eta_2 I_0)(S + \theta V_1)}{N} + \beta_1 U S - \sigma E - \mu E, \\
\frac{dI_a}{dt} &= \psi\sigma E - \gamma_1 I_a - \mu I_a, \\
\frac{dI}{dt} &= (1 - \psi - \phi)\,\sigma E - \gamma_2 I - \delta_1 I - \mu I, \\
\frac{dI_0}{dt} &= \phi\sigma E - \gamma_3 I_0 - \delta_2 I_0 - \mu I_0, \\
\frac{dV_1}{dt} &= \nu_1 S - \nu_2 V_1 - \omega_1 V_1 - \frac{\beta(\eta_1 I + I_a + \eta_2 I_0)\theta V_1}{N} - \mu V_1, \\
\frac{dV_2}{dt} &= \nu_2 V_1 - \gamma_4 V_2 - \mu V_2, \\
\frac{dR}{dt} &= \gamma_2 I + \gamma_1 I_a + \gamma_3 I_0 + \gamma_4 V_2 - \chi R - \mu R, \\
\frac{dU}{dt} &= \theta_2 I + \theta_1 I_a + \theta_3 I_0 - \epsilon U.
\end{cases}
\tag{1}
$$

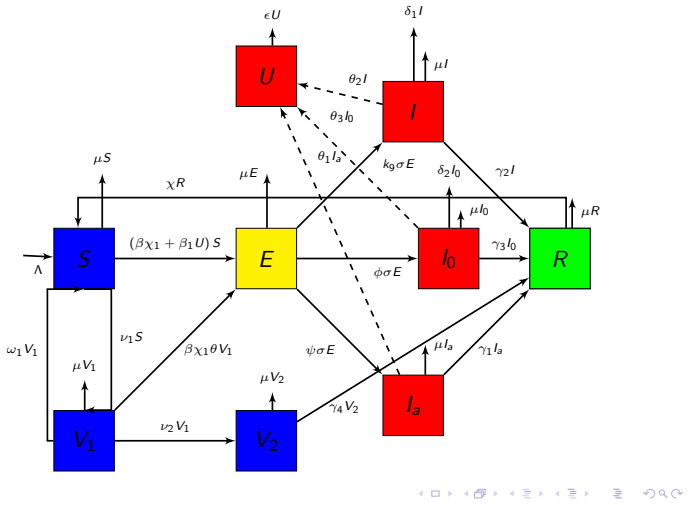

Figure 1: Flow diagram

A schematic representation of the model described by (1) is illustrated in Figure 1. The model begins with the following initial conditions:

$$S(0) = S_0 > 0, \quad E(0) \geq 0, \quad I_a(0) \geq 0, \quad I(0) \geq 0, \quad I_0(0) \geq 0,$$

$$V_1(0) = V_{10} > 0, \quad V_2(0) = V_{20} > 0, \quad R(0) \geq 0, \quad U(0) \geq 0.$$

To simplify notation, we define the following constants:

$$\begin{aligned}
&k_1 = \nu_1 + \mu, && k_2 = \mu + \sigma, && k_3 = \gamma_1 + \mu,\\
&k_4 = \gamma_2 + \delta_1 + \mu, && k_5 = \gamma_3 + \delta_2 + \mu, && k_6 = \nu_2 + \omega_1 + \mu,\\
&k_7 = \gamma_4 + \mu, && k_8 = \chi + \mu, && k_9 = 1 - \phi - \psi,\\
&\chi_1 = \frac{\eta_1 I + I_a + \eta_2 I_0}{N}.
\end{aligned}$$

Accordingly, the system governed by (1) can be rewritten as follows:

$$\begin{cases} \frac{dS}{dt} &= \Lambda - \frac{\beta(\eta_1 I + I_a + \eta_2 I_0)S}{N} - \beta_1 US + \omega_1 V_1 + \chi R - k_1 S, \\ \frac{dE}{dt} &= \frac{\beta(\eta_1 I + I_a + \eta_2 I_0)(S + \theta V_1)}{N} + \beta_1 US - k_2 E, \\ \frac{dI_a}{dt} &= \psi\sigma E - k_3 I_a, \\ \frac{dI}{dt} &= k_9\sigma E - k_4 I, \\ \frac{dI_0}{dt} &= \phi\sigma E - k_5 I_0, \\ \frac{dV_1}{dt} &= \nu_1 S - \frac{\beta(\eta_1 I + I_a + \eta_2 I_0)\theta V_1}{N} - k_6 V_1, \\ \frac{dV_2}{dt} &= \nu_2 V_1 - k_7 V_2, \\ \frac{dR}{dt} &= \gamma_2 I + \gamma_1 I_a + \gamma_3 I_0 + \gamma_4 V_2 - k_8 R, \\ \frac{dU}{dt} &= \theta_2 I + \theta_1 I_a + \theta_3 I_0 - \epsilon U. \end{cases} \tag{2}$$

Table 1: Parameters and their meanings in relation to system (1)

Parameters	Description
Λ	Recruitment rate
$1/\chi$	Average duration of immunity before waning
θ_1	Viral shedding rate by asymptomatic individuals
θ_2	Viral shedding rate by symptomatic individuals
θ_3	Viral shedding rate by Omicron-infected individuals
ω_1	Rate of loss of vaccine-induced immunity
η_1	Adjustment parameter
η_2	Adjustment parameter
$1/\sigma$	Latent period
ψ	Modification parameter
ϕ	Fraction of exposed individuals showing symptoms
ϵ	Decline rate of viral viability over time in contaminated surroundings
δ_1	Mortality rate due to disease in non-Omicron-infected individuals
δ_2	Disease-induced death rate of Omicron-infected individuals
γ_1	Recovery rate for asymptomatic individuals
μ	Natural mortality rate
β	The rate at which the infection spreads
β_1	The highest rate of spread caused by environmental contamination
ν_1	Vaccination rate (dose I)
ν_2	Vaccination rate (dose II)
γ_2	Rate of recovery in those exhibiting symptoms
γ_3	Recovery rate for Omicron-infected individuals
γ_4	Rate of progression to immune class as a result of receiving the second dose of the vaccine
θ	Relative risk of infection for vaccinated individuals with the dose I

Table 2: Model (1) calibration values

Parameters	Range	Baseline	Sources
β	$(0.2, 0.8999)\ day^{-1}$	0.6594	[52]
β_1	$(0, 0.000105)\ day^{-1}$	0.000104	[40]
ν_1	$(0, 1)\ day^{-1}$	0.0215	[55]
ν_2	$(0, 1)\ day^{-1}$	0.0341	[55]
γ_1	$(0.1, 0.5)\ day^{-1}$	0.3899	Estimated
γ_2	$(0.001, 0.2)\ day^{-1}$	0.069	Estimated
γ_3	$(0.01, 0.3)\ day^{-1}$	0.1746	Estimated
γ_4	$(0.1, 0.9)\ day^{-1}$	0.84	[17]
δ_1	$(0, 0.1)\ day^{-1}$	0.08	Estimated
δ_2	$(0, 0.09)\ day^{-1}$	0.0015	Estimated
ψ	$(0.9, 0.98)\ day^{-1}$	0.9566	[20]
ϕ	$(0.01, 0.02)\ day^{-1}$	0.0101	[20]
Λ	$(10, 50000)\ day^{-1}$	1319.294	[1]
μ	$(0, 0.00042)\ day^{-1}$	0.000042578	[1]
θ_1	$(0, 0.0000021)\ day^{-1}$	0.0000012	[40]
θ_2	$(0, 0.00013)\ day^{-1}$	0.00011	[40]
θ_3	$(0, 0.001)\ day^{-1}$	0.0001	Assumed
ϵ	$(0, 0.1)\ day^{-1}$	0.09	[40]
σ	$(0.2, 0.9)\ day^{-1}$	0.8999	[20]
ω_1	$(0, 0.61)\ day^{-1}$	0.1224	[17]
χ		$0.0027\ day^{-1}$	Assumed
η_1	$(0.45, 0.9)$	0.78	[20, 13]
η_2	$(0.35, 0.77)$	0.49	[20, 13]
θ	$(0.01, 0.5)\ day^{-1}$	0.315	[56]

3 Mathematical analysis

In this section, we present key analytical insights for the model (2), including the positivity and boundedness of its solutions, the existence of both disease-free and endemic equilibria, and an analysis of their stability with respect to the control reproduction number.

3.1 Nonnegativity and boundedness

This section shows that the solutions to the model system (1) remain both nonnegative and bounded.

$\frac{dS}{dt}\big|_{S=0} = \Lambda + \omega_1 V_1 + \chi R > 0,$ $\quad \frac{dE}{dt}\big|_{E=0} = \frac{\beta(\eta_1 I + I_a + \eta_2 I_0)S}{N} + \beta_1 US \geq 0,$

$\frac{dI_a}{dt}\big|_{I_a=0} = \psi\sigma E \geq 0,$ $\quad \frac{dI}{dt}\big|_{I=0} = k_9\sigma E \geq 0,$ $\quad \frac{dI_0}{dt}\big|_{I_0=0} = \phi\sigma E \geq 0,$

$\frac{dV_1}{dt}\big|_{V_1=0} = \nu_1 S > 0,$ $\quad \frac{dV_2}{dt}\big|_{V_2=0} = \nu_2 V_1 > 0,$

$\frac{dR}{dt}\big|_{R=0} = \gamma_2 I + \gamma_1 I_a + \gamma_3 I_0 + \gamma_4 V_2 > 0, \quad \frac{dU}{dt}\big|_{U=0} = \theta_2 I + \theta_1 I_a + \theta_3 I_0 \geq 0.$

Since all the rates in the system are nonnegative, starting within the interior of the nonnegative cone R^9_+ ensures the system's trajectory remains inside it. This is because the vector field points inward along every boundary surface, guaranteeing that none of the solutions to system (1) will become negative.

To demonstrate that the solutions are bounded, we consider the full system (1), leading to the equation:

$$\frac{dN}{dt} = \Lambda - \mu N - \delta_1 I - \delta_2 I_0.$$

Since $\delta_1 I + \delta_2 I_0 \geq 0$, it follows that

$$\frac{dN}{dt} < \Lambda - \mu N.$$

From [7], we conclude as $t \to \infty$ that

$$0 \leq N(t) \leq \frac{\Lambda}{\mu} = N_0.$$

Because $I(t), I_0, I_a \leq N(t)$ at any time, we also have

$$I(t), I_0, I_a \leq \frac{\Lambda}{\mu}.$$

Next, from (1), we derive

$$\frac{dU}{dt} = \theta_2 I + \theta_1 I_a + \theta_3 I_0 - \epsilon U \leq (\theta_2 + \theta_1 + \theta_3)\frac{\Lambda}{\mu} - \epsilon U.$$

Since $0 \leq U(0)$, applying Gronwall's inequality yields

$$U(t) \leq \frac{(\theta_2 + \theta_1 + \theta_3)\Lambda}{\epsilon\mu}.$$

Hence the feasible region for the model system (1) is

$$\Theta = \left\{ (S, E, I_a, I, I_0, V_1, V_2, R, U) \in R^9_+ : \right.$$
$$0 \leq S, E, I_a, I, I_0, V_1, V_2, R, N \leq \frac{\Lambda}{\mu},$$
$$\left. 0 \leq U \leq \frac{(\theta_2 + \theta_1 + \theta_3)\,\Lambda}{\epsilon\mu} \right\}.$$

The preceding analysis of nonnegativity and boundedness leads to the following conclusion.

Theorem 1. Under the given initial conditions, the system's solutions remain nonnegative for all future times. Moreover, this closed region is positively invariant under the flow of the model system (1).

3.2 Disease-free equilibrium and control reproduction number

To determine the model's control reproduction number R_c, we apply the next-generation matrix method as outlined in [53]. This yields

$$\begin{aligned}\mathcal{R}_c =& \frac{1}{k_2k_3k_4k_5(r_0+S_0+V_{10}+V_{20})\epsilon}\sigma(\beta\epsilon(S_0+V_{10}\theta)c_1\\ &+S_0(r_0+S_0+V_{10}+V_{20})\beta_1c_2),\end{aligned}$$

where

$$c_1 = (k_3k_5k_9\eta_1 + k_4k_3\eta_2\phi + k_4k_5\psi),$$

$$c_2 = (k_3k_5k_9\theta_2 + k_4k_3\theta_3\phi + k_4k_5\theta_1\psi),$$

$$c_3 = (k_3k_5k_9\gamma_2 + k_4k_3\gamma_3\phi + k_4k_5\gamma_1\psi),$$

$$\phi = \frac{\beta(S_0+\theta V_{10})}{r_0+S_0+V_{10}+V_{20}}.$$

Additionally, the model (2) admits the disease-free equilibrium (DFE),
$\zeta_0 = (S_0, 0, 0, 0, 0, V_{10}, V_{20}, r_0, 0)$. The components of the DFE are given by

$$S_0 = \left(\frac{\Lambda k_6k_7k_8}{\mu k_6k_7k_8 + \mu\nu_1(\gamma_4(\mu+\nu_2+\chi)+k_8(\mu+\nu_2))}\right),$$

$$V_{10} = \frac{\nu_1S_0}{k_6}, \qquad V_{20} = \frac{\nu_1\nu_2S_0}{k_6k_7},$$

$$r_0 = \frac{\gamma_4\nu_1\nu_2S_0}{k_6k_7k_8}, \qquad N^0 = S_0+V_{10}+V_{20}+r_0.$$

In the absence of any intervention and vaccinations, $\nu_1 = 0, \nu_2 = 0, \omega_1 = 0, \theta = 0$, implies $V_{10} = V_{20} = r_0 = 0, S_0 = \frac{\Lambda}{\mu} = N_0$. Hence, the basic reproduction number R_0 of the model (2) is given by

$$R_0 = \frac{\sigma\beta c_1}{k_2k_3k_4k_5} + \frac{\sigma\beta_1 N_0 c_2}{k_2k_3k_4k_5\epsilon}. \tag{3}$$

It is clear that

$$R_c = \frac{\sigma\beta c_1}{k_2k_3k_4k_5}\frac{S_0 + V_{10}\theta}{N^0} + \frac{\sigma\beta_1 c_2}{k_2k_3k_4k_5\epsilon}S_0.$$

Since $\frac{S_0}{N^0} \leq 1$ and $0 \leq \frac{S_0+V_{10}\theta}{N^0} \leq 1$, this implies that $R_c \leq R_0$.

Theorem 2. The DFE ζ_0 of the system (2) is locally asymptotically stable if $R_c < 1$ and unstable if $R_c > 1$.

3.3 Existence and stability of the endemic equilibria

We define the endemic equilibrium

$$\zeta^* = \left(S^*, E^*, I_a^*, I^*, I_0^*, V_1^*, V_2^*, R^*, U^*\right)$$

of system (2) as a steady state with all infected components strictly positive. From the equilibrium conditions, we obtain

$$E^* = b_1 I^*, \qquad I_a^* = b_2 I^*, \qquad I_0^* = b_3 I^*, \qquad U^* = b_4 I^*, \qquad V_2^* = \frac{\nu_2 V_1^*}{k_7},$$
$$R^* = \frac{\gamma_2 I^* + \gamma_1 I_a^* + \gamma_3 I_0^* + \gamma_4 V_2^*}{k_8},$$

where

$$N^* = S^* + E^* + I_a^* + I^* + I_0^* + V_1^* + V_2^* + R^*$$

and

$$b_1 = \frac{k_4}{k_9\sigma}, \qquad b_2 = \frac{b_1\sigma\psi}{k_3}, \qquad b_3 = \frac{b_1\sigma\phi}{k_5}, \qquad b_4 = \frac{b_2\theta_1 + b_3\theta_3 + \theta_2}{\epsilon}.$$

Substituting these expressions into the remaining equilibrium equations reduces the problem to a system of three coupled nonlinear algebraic equations in the unknowns S^*, I^* and V_1^*. The coefficients of these equations can be written in terms of auxiliary quantities such as

$$b_5 = b_2\gamma_1 + \gamma_2 + b_3\gamma_3,$$
$$b_6 = b_5k_7 + (1 + b_1 + b_2 + b_3)k_7k_8,$$
$$b_7 = k_7k_8,$$

$$
\begin{aligned}
b_8 &= k_7k_8 + k_8\nu_2 + \gamma_4\nu_2,\\
b_9 &= b_2 + \eta_1 + b_3\eta_2,\\
g_1 &\equiv \Lambda + \frac{(b_5k_7I^* + \gamma_4\nu_2V_1^*)\,\xi}{b_7} + \omega_1V_1^*\\
&\quad - \left(k_1 + b_4\beta_1I^* + \frac{b_7\beta b_9I^*}{b_6I^* + b_7S^* + b_8V_1^*}\right)S^* = 0,\\
g_2 &\equiv -b_1k_2 + b_4\beta_1S^* + \frac{b_7\beta b_9(S^* + V_1^*\theta)}{b_6I^* + b_7S^* + b_8V_1^*} = 0,\\
g_3 &\equiv \nu_1S^* - V_1^*\left(k_6 + \frac{b_7\beta b_9\theta I^*}{b_6I^* + b_7S^* + b_8V_1^*}\right) = 0.
\end{aligned}
$$

This process yields a system of three nonlinear algebraic equations in the steady-state variables S^*, I^*, and V_1^*:

$$g_1(S^*, I^*, V_1^*) = 0, \qquad g_2(S^*, I^*, V_1^*) = 0, \qquad g_3(S^*, I^*, V_1^*) = 0.$$

The resulting equations are highly nonlinear and contain rational terms, making analytical manipulation and the derivation of explicit solutions extremely challenging. Consequently, deriving closed-form expressions for the equilibrium (S^*, I^*, V_1^*) or establishing simple algebraic conditions that guarantee the existence or uniqueness of a positive endemic equilibrium is highly difficult. Therefore, the equilibrium values are computed numerically. For the parameter values given in Table 2, the control reproduction number $R_c = 1.50(> 1)$. Solving numerically, the system $(g_1, g_2, g_3) = (0, 0, 0)$ yields a unique positive endemic equilibrium $\zeta^* = \big(29503, 523, 772, 147, 23, 877, 42, 15575, 0.274\big)$.

Moreover, we study the occurrence of a transcritical bifurcation by applying the center manifold theory [8]. For convenience, we perform the change of variables

$$S = x_1 + S_0, \quad E = x_2, \quad I_a = x_3, \quad I = x_4, \quad I_0 = x_5,$$

$$V_1 = x_6 + V_{10}, \quad V_2 = x_7 + V_{20}, \quad R = x_8 + r_0, \quad U = x_9.$$

With this transformation, the model system (1) can be written in the following compact form:

$$\begin{cases} \frac{dx_1}{dt} &= \Lambda - \frac{\beta(\eta_1 x_4+x_3+\eta_2 x_5)(x_1+S_0)}{N+(S_0+V_{10}+V_{20}+r_0)} - \beta_1(x_1+S_0)x_9 + \chi(r_0+x_8) \\ & \quad +\omega_1(x_6+V_{10}) - k_1(x_1+S_0), \\ \frac{dx_2}{dt} &= \frac{\beta(\eta_1 x_4+x_3+\eta_2 x_5)((x_1+S_0)+\theta(x_6+V_{10}))}{N+(S_0+V_{10}+V_{20}+r_0)} + \beta_1(x_1+S_0)x_9 - k_2 x_2, \\ \frac{dx_3}{dt} &= \sigma\psi x_2 - k_3 x_3, \\ \frac{dx_4}{dt} &= \sigma k_9 x_2 - k_4 x_4, \\ \frac{dx_5}{dt} &= \sigma\phi x_2 - k_5 x_5, \\ \frac{dx_6}{dt} &= \nu_1(x_1+S_0) - \frac{\theta\beta(\eta_1 x_4+x_3+\eta_2 x_5)(x_6+V_{10})}{N+(S_0+V_{10}+V_{20}+r_0)} - k_6(x_6+V_{10}), \\ \frac{dx_7}{dt} &= \nu_2(x_6+V_{10}) - k_7(x_7+V_{20}), \\ \frac{dx_8}{dt} &= \gamma_2 x_4 + \gamma_1 x_3 + \gamma_3 x_5 + \gamma_4(x_7+V_{20}) - k_8(r_0+x_8), \\ \frac{dx_9}{dt} &= \theta_1 x_3 + \theta_2 x_4 + \theta_3 x_5 - \epsilon x_9. \end{cases} \tag{4}$$

At the corresponding DFE ζ_0, the Jacobian of the system (4) is expressed as follows:

$$J_{\zeta_0} = \begin{bmatrix} -k_1 & 0 & -k_{10} & -k_{10}\eta_1 & -k_{10}\eta_2 & \omega_1 & 0 & \chi & -S_0\beta_1 \\ 0 & -k_2 & k_{11} & k_{11}\eta_1 & k_{11}\eta_2 & 0 & 0 & 0 & S_0\beta_1 \\ 0 & \sigma\psi & -k_3 & 0 & 0 & 0 & 0 & 0 & 0 \\ 0 & \sigma k_9 & 0 & -k_4 & 0 & 0 & 0 & 0 & 0 \\ 0 & \sigma\phi & 0 & 0 & -k_5 & 0 & 0 & 0 & 0 \\ \nu_1 & 0 & -k_{12} & -k_{12}\eta_1 & -k_{12}\eta_2 & -k_6 & 0 & 0 & 0 \\ 0 & 0 & 0 & 0 & 0 & \nu_2 & -k_7 & 0 & 0 \\ 0 & 0 & \gamma_1 & \gamma_2 & \gamma_3 & 0 & \gamma_4 & -k_8 & 0 \\ 0 & 0 & \theta_1 & \theta_2 & \theta_3 & 0 & 0 & 0 & -\epsilon \end{bmatrix},$$

where

$$k_{10} = \frac{S_0\beta_c}{(S_0+V_{10}+V_{20}+r_0)}, \quad k_{11} = \frac{\beta_c(S_0+V_{10}\theta)}{(S_0+V_{10}+V_{20}+r_0)}, \quad k_{12} = \frac{V_{10}\beta_c\theta}{(S_0+V_{10}+V_{20}+r_0)}.$$

Assuming $R_c = 1$, we determine the critical value β_c of the bifurcation parameter β, given by

$$\beta_c = -\frac{(r_0+S_0+V_{10}+V_{20})\,(-k_2k_3k_4k_5\epsilon + S_0\beta_1\sigma c_2)}{\epsilon(S_0+V_{10}\theta)\sigma c_1}.$$

It can be easily verified that the Jacobian at $\beta = \beta_c$ has a right eigenvector (corresponding to the zero eigenvalue) given by $W = (w_1, w_2, w_3, w_4, w_5, w_6, w_7, w_8, w_9)^T$, where

$$w_2 = 1, \quad w_3 = \frac{\sigma\psi}{k_3}, \quad w_4 = \frac{k_9\sigma}{k_4}, \quad w_5 = \frac{\sigma\phi}{k_5},$$

$$w_9 = \frac{\sigma c_2}{k_3k_4k_5\epsilon}, \quad w_6 = \frac{\nu_1 w_1}{k_6} - \frac{c_1k_{12}\sigma}{k_3k_4k_5k_6}, \quad w_7 = \frac{\nu_2(k_3k_4k_5w_1\nu_1 - c_1k_{12}\sigma)}{k_3k_4k_5k_6k_7},$$

$$w_1 = -\frac{\sigma(c_2k_6k_7k_8s_0\beta_1 - c_3k_6k_7\epsilon\chi + c_1\epsilon(k_{10}k_6k_7k_8 + k_{12}(\gamma_4\nu_2\chi + k_7k_8\omega_1)))}{k_3k_4k_5\epsilon(k_1k_6k_7k_8 - \nu_1(\gamma_4\nu_2\chi + k_7k_8\omega_1))},$$

$$w_8 = \frac{\sigma(-\gamma_4\nu_2(c_2s_0\beta_1\nu_1 + c_1\epsilon(k_1k_{12} + k_{10}\nu_1)) + c_3\varepsilon(k_1k_6k_7 - \nu_1(k_7\omega_1)))}{k_3k_4k_5\epsilon(k_1k_6k_7k_8 - \nu_1(\gamma_4\nu_2\chi + k_7k_8\omega_1))}.$$

The components of the left eigenvector, associated with the zero eigenvalue, are $V = (v_1, v_2, v_3, v_4, v_5, v_6, v_7, v_8, v_9)$, which must fulfill the conditions $V.J = 0$ and $V.W = 1$. Solving these, we obtain

$$v_1 = 0, \quad v_6 = 0, \quad v_7 = 0, \quad v_8 = 0, \quad v_9 = \frac{\beta_1S_0v_2}{\epsilon}, \quad v_3 = \frac{v_2(k_{11}\epsilon + \beta_1\theta_1S_0)}{k_3\epsilon},$$

$$v_4 = \frac{v_2(k_{11}\epsilon\eta_1 + \beta_1\theta_2S_0)}{k_4\epsilon}, \quad v_5 = \frac{v_2(k_{11}\epsilon\eta_2 + \beta_1\theta_3S_0)}{k_5\epsilon}, \quad v_2 = \frac{k_3^2k_4^2k_5^2\epsilon^2}{m_5},$$

where

$$\begin{aligned} m_5 &= c_2k_3k_4k_5S_0\beta_1\sigma + k_4^2k_5^2\epsilon(k_{11}\epsilon + S_0\beta_1\theta_1)\sigma\psi \\ &\quad + k_3^2\epsilon(k_5^2k_9(k_{11}\epsilon\eta_1 + S_0\beta_1\theta_2)\sigma + k_4^2(k_5^2\epsilon + k_{11}\epsilon\eta_2\sigma\phi + S_0\beta_1\theta_3\sigma\phi)), \\ m_6 &= (w_3 + w_4\eta_1 + w_5\eta_2). \end{aligned}$$

The bifurcation coefficients a and b, as given in [8, Theorem 4.1], are computed using the formulas below:

$$\begin{aligned} a &= \sum_{k,i,j=1}^{9} v_kw_iw_j\frac{\partial^2 f_k}{\partial x_i\partial x_j}(0,0) \\ &= \frac{1}{N_0^2}2(v_2)(r_0{}^2w_1w_9\beta_1 + S_0{}^2w_1w_9\beta_1 \\ &\quad + ((v_{10} + v_{20})w_1\left((v_{10} + v_{20})w_9\beta_1 + \beta_cm_6\right) \\ &\quad + r_0w_1\left(2(s_0 + v_{10} + v_{20})w_9\beta_1 + \beta_c(w_3 + w_4\eta_1 + w_5\eta_2)\right) + r_0w_6\beta_cm_6\theta \\ &\quad - (-v_{20}w_6 + v_{10}(w_1 + w_2 + w_3 + w_4 + w_5 + w_7 + w_8))\beta_cm_6\theta \\ &\quad + S_0\left(2(v_{10} + v_{20})w_1w_9\beta_1\right. \\ &\quad \left.-\beta_cm_6(w_2 + w_3 + w_4 + w_5 + w_6 + w_7 + w_8 - w_6\theta)\right). \end{aligned}$$

$$
\begin{aligned}
b &= \sum_{k,i,j=1}^{9} v_k w_i \frac{\partial^2 f_k}{\partial x_i \partial \beta}(0,0) \\
&= v_2 \left(\frac{w_3(S_0 + V_{10}\theta)}{r_0 + S_0 + V_{10} + V_{20}} + \frac{w_4\eta_1(S_0 + v_{10}\theta)}{r_0 + S_0 + V_{10} + V_{20}} + \frac{w_5\eta_2(S_0 + V_{10}\theta)}{r_0 + S_0 + V_{10} + V_{20}} \right).
\end{aligned}
$$

Given that $a < 0$ and $b > 0$ when $\beta = \beta_c$, [8, Theorem 4.1 and Remark 1] implies the presence of a transcritical bifurcation at $R_c = 1$. Consequently, the endemic equilibrium point is locally asymptotically stable for values of R_c exceeding 1.

3.4 Global stability of DFE

This section examines the global stability of the DFE.

Theorem 3. If $R_c < 1$, the DFE ζ_0 in model (2) is globally asymptotically stable, whereas it becomes unstable when $R_c > 1$.

Proof. We construct an appropriate Lyapunov function to demonstrate the global stability of the DFE ζ_0,

$$
\mathcal{G} = a_1 E + a_2 I_a + a_3 I + a_4 I_0 + a_5 U, \tag{5}
$$

The nonnegative constants a_j for $j = 1, 2, \ldots, 5$ will be specified later. Moreover, by substituting the expressions from model (2) and differentiating (5), we arrive at the following result:

$$
\begin{aligned}
\mathcal{G}' &= a_1 E' + a_2 I_a' + a_3 I' + a_4 I_0' + a_5 U' \\
&= a_1 \left(\frac{\beta(\eta_1 I + I_a + \eta_2 I_0)(S + \theta V)}{N} + \beta_1 S U - k_2 E \right) + a_2(\sigma\psi E - k_3 I_a) \\
&\quad + a_3(\sigma k_9 E - k_4 I) + a_4(\sigma\phi E - k_5 I_0) + a_5(\theta_1 I_a + \theta_2 I + \theta_3 I_0 - \epsilon U) \\
&\leq a_1 \left(\frac{\beta(\eta_1 I + I_a + \eta_2 I_0)(S_0 + \theta V_{10})}{N^0} + \beta_1 S_0 U - k_2 E \right) + a_2(\sigma\psi E - k_3 I_a) \\
&\quad + a_3(\sigma k_9 E - k_4 I) + a_4(\sigma\phi E - k_5 I_0) + a_5(\theta_1 I_a + \theta_2 I + \theta_3 I_0 - \epsilon U) \\
&= \left(-a_1 k_2 + a_2\sigma\psi + a_3 k_9 \sigma + a_4 \sigma\phi\right) E + \left(\frac{\beta a_1 (S_0 + \theta V_{10})}{N^0} - a_2 k_3 + a_5 \theta_1 \right) I_a \\
&\quad + \left(\frac{\beta a_1 \eta_1 (S_0 + \theta V_{10})}{N^0} - a_3 k_4 + a_5 \theta_2 \right) I \\
&\quad + \left(\frac{\beta a_1 \eta_2 (S_0 + \theta V_{10})}{N^0} - a_4 k_5 + a_5 \theta_3 \right) I_0 + \left(\frac{a_1(\beta_1 \Lambda)}{\mu p} - a_5 \epsilon \right) U.
\end{aligned} \tag{6}
$$

We will assign the constants the following values:

$$a_1 = \frac{k_5 N^0 \epsilon}{S_0\beta\epsilon\eta_2 + V_{10}\beta\epsilon\eta_2\theta + N^0 S_0\beta_1\theta_3}, \quad a_4 = 1, \quad a_5 = \frac{(a_1 S_0\beta_1)}{\epsilon},$$

$$N^0 = S_0 + V_{10} + V_{20} + r_0,$$

$$a_2 = \frac{(a_1 S_0\beta\epsilon + a_1 V_{10}\beta\epsilon\theta + a_1 N^0 S_0\beta_1\theta_1)}{k_3 N^0\epsilon},$$

$$a_3 = \frac{(a_1 S_0\beta\epsilon\eta_1 + a_1 V_{10}\beta\epsilon\theta\eta_1 + a_1 N^0 S_0\beta_1\theta_2)}{k_4 N^0\epsilon}.$$

Utilizing inequality (6), we obtain the result below:

$$\mathcal{G}' \leq \left(\frac{k_2 k5 N^0(R_c - 1)\epsilon}{\beta\epsilon\eta_2(S_0 + V_{10}\theta) + N^0 S_0\beta_1\theta_3}\right) E. \tag{7}$$

Hence, $\mathcal{G}' \leq 0$ whenever $R_c < 1$, and equality holds only when $E = 0$. By LaSalle's invariance principle, ζ_0 is globally asymptotically stable for $R_c < 1$. □

4 Numerical simulation

4.1 Estimation of the model parameters

In this section, we calibrate the proposed model using real-world data to gain a deeper understanding of the pandemic's transmission dynamics.

To begin, baseline parameter values are established by analyzing publicly available COVID-19 data, relevant datasets, and verified sources from the literature. Recent evidence indicates that the mean intervals between successive SARS-CoV-2 infections are approximately 204.4±51.1 days for the Alpha variant, 291.2 ± 58.2 days for the Delta variant, and 361.2 ± 131.6 days for the Omicron variant [30]. As the present study investigates the Omicron outbreak, the average period of immunity acquired following infection is taken to be $1/\chi = 361$ days. Specifically, we utilize data on the total reported COVID-19 cases in India spanning the period from 30 December 2021 to 30 April 2022 [16].

Model fitting is performed using the least squares method [25], which minimizes the discrepancies between observed data points, Y_i, and corresponding model estimates, X_i. The objective is to reduce the sum of squared errors (SSE) between the observed and predicted values, defined as

$$SSE = \sum_{i=1}^{n} (Y_i - X_i)^2.$$

In Figure 2, the continuous curve represents the fitted model, while the star-shaped markers denote the actual reported daily confirmed cases. From this calibration, the control reproduction number is estimated as $R_c = 1.17$, indicating that the Omicron variant retains a high potential for rapid transmission.

Overall, the simulated results align well with the observed data, validating the model's performance. The corresponding parameter estimates are summarized in Table 2.

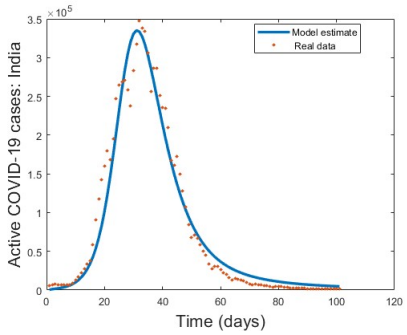

Figure 2: Fitted curve of confirmed cases in India for proposed model [16]

4.2 Sensitivity analysis

Investigating the influence of various parameters on the control reproduction number, R_c, is fundamental to understanding the behaviour of infectious diseases. This type of analysis enables the identification of key contributors to disease transmission and facilitates the formulation of effective intervention strategies during epidemics. The normalized forward sensitivity index of a parameter p with respect to R_c is expressed as (see [25])

$$\Gamma_{R_c}^{p} = \frac{\partial R_c}{\partial p} \cdot \frac{p}{R_c}.$$

.

The sensitivity indices for R_c, computed using parameter values from Table 2, are listed in Table 3. The results indicate that increases in parameters such as $\beta, \omega_1, \sigma, \mu, \eta_1, \eta_2, \beta_1, \Lambda, \chi, \theta_1, \theta_2, \theta_3$, and γ_4 lead to an increase in R_c. In contrast, parameters like $\psi, \phi, \nu_1, \nu_2, \epsilon, \delta_1, \delta_2, \gamma_1, \gamma_2, \gamma_3$ are associated with a reduction in R_c. As shown in Figure 3(a), the parameter χ exerts the most

significant positive effect, whereas ψ has the most notable negative effect on R_c. Since lower values of R_c are desirable to control disease spread, it is advisable to increase the parameters with negative indices and reduce those with positive indices.

To assess how different parameters affect the infected population $I(t)$, a sensitivity analysis of the model described by (1) is performed using the PRCC method and the Latin hypercube sampling (LHS) strategy, as outlined in [**?**]. The analysis assumes a uniform distribution for all model parameters, with $I(t)$ serving as the response function. The PRCC values provide insight into the strength and direction of the relationship between each parameter and $I(t)$, thus highlighting the most influential parameters. Figure 3(b) displays the PRCC results obtained from 500 simulation runs.

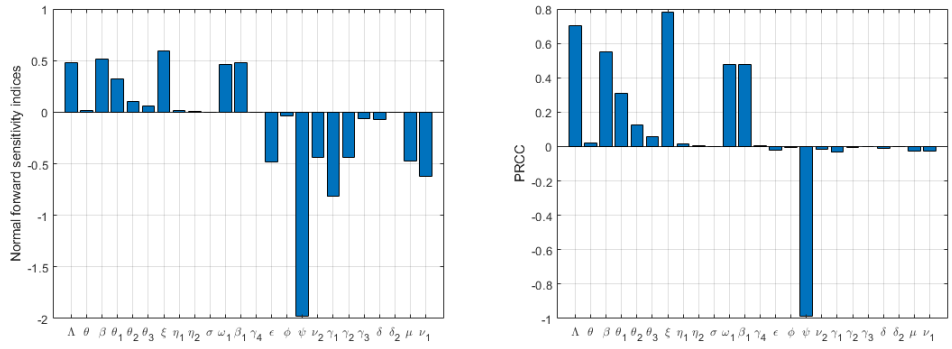

(a) Normalized forward sensitivity indices $\Gamma^p_{R_c}$ (b) PRCC sensitivity indices of $I(t)$

Figure 3: Sensitivity analyses of the model parameters as in Table 1

Figure 4 presents a 2-D contour plot, while Figure 5 illustrates a 3-D contour plot of R_c as a function of vaccination rates for dose I (ν_1) and dose II (ν_2). Both figures indicate that as vaccination rates increase over time, the incidence of COVID-19 declines sharply.

4.3 Impact of vaccination

To investigate the impact of the first dose of the vaccine (Dose I) on the infected population, a numerical simulation is conducted for varying vaccination rates, denoted by ν_1, as illustrated in Figure 6(a). Similarly, the impact of the second dose on the infected population I is presented in Figure 6(b) for different levels of ν_2. Without the second dose, the number of infected individuals experiences a significant surge. However, with an increase in the administration of the second

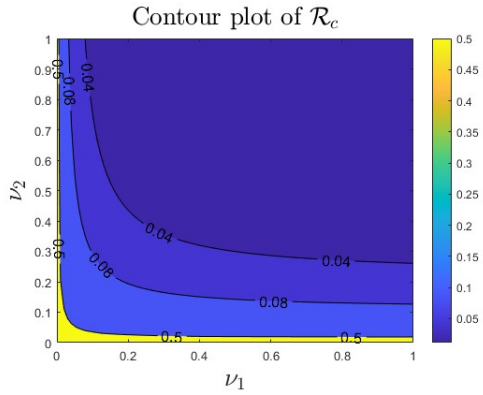

Figure 4: $2D$ contour plot of R_c as a function of ν_1 and ν_2

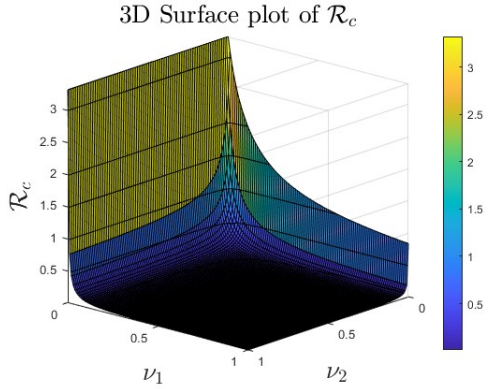

Figure 5: $3D$ contour plot of R_c as a function of ν_1 and ν_2

Table 3: Normalized sensitivity indices of R_c with respect to the model parameters in (1), for parameter values given in Table 2

Parameter	Sensitivity indices	Parameter	Sensitivity indices	Parameter	Sensitivity indices
Λ	0.481054	η_2	0.00559502	γ_1	-0.818185
θ	0.0185693	σ	0.0000473119	γ_4	0.00252367
β	0.518946	ω_1	0.460218	δ_1	-0.0715937
θ_1	0.318524	β_1	0.481054	ν_1	-0.624311
θ_2	0.101881	ϵ	-0.481054	γ_2	-0.0438512
θ_3	0.0606476	ϕ	-0.0369766	γ_3	-0.0656625
χ	0.588956	ψ	-1.97258	μ	-0.471738
η_1	0.0136015	ν_2	-0.436894	δ_2	-0.00056411

dose, there is a noticeable and sharp decline in the infected population. After receiving dose I of the vaccination, we observe a significant decrease in the infected population I, as shown in

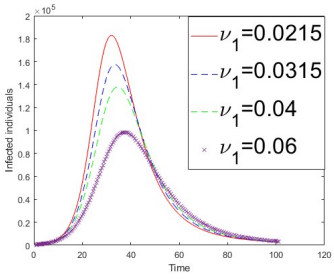

(a) Effect of ν_1 on I

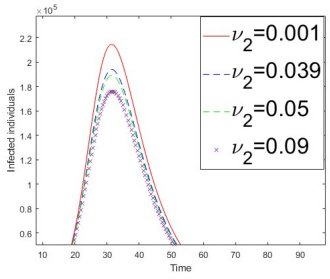

(b) Effect of ν_2 on I, where $\nu_1 = 0.01$

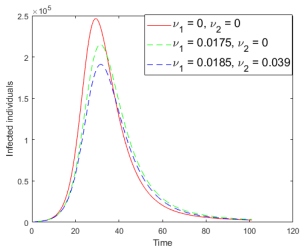

(c) Effect of ν_1 and ν_2 on I

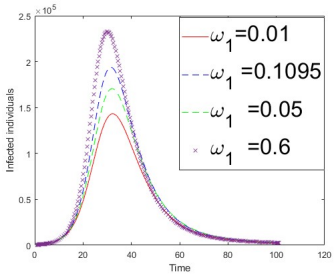

(d) Effect of ω_1 on I

Figure 6: The effects of varying ω_1, ν_1, and ν_2 on the infected population I

Figure 6(c). This decrease is even more pronounced after receiving dose II, compared to dose I, as shown in Figure 6(c). Asymptomatic patients have a higher rate of infectiousness, so their impact on the infection levels I is illustrated in Figure 7(c) for different levels of ψ. This is likely due to the fact that individuals in this group are often unaware of their COVID-19 infection and, as a result, may not consistently adhere to measures aimed at preventing transmission.

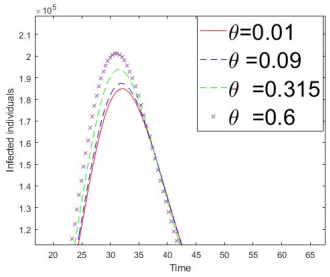

(a) Effect of θ on I

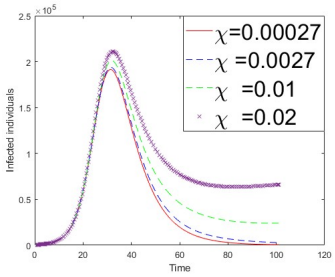

(b) Effect of χ on I

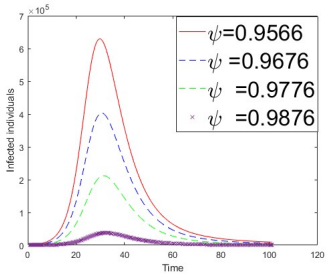

(c) Effect of ψ on I

Figure 7: The effects of varying ψ, χ, θ on the infected population I

4.4 Impact of environmental contamination

Environmental contamination has been identified as a key factor contributing to the transmission of COVID-19. Studies have shown that the virus remains viable on various surfaces for differing durations—up to 4 hours on copper, 24 hours on cardboard, and as long as 72 hours on stainless steel and plastic [54]. The proposed mathematical model (1) incorporates the effects of environmental contamination, particularly from infected individuals categorized in the I_a, I, and I_0 compartments.

We analyzed the impact of environmental contamination on the dynamics of the proposed model. The time series in Figure 8 illustrates how parameters related to environmental contamination affect infection levels. When the rates of environmental contamination (θ_1, θ_2, and θ_3) increase, the infected population correspondingly rises, as shown in Figures 8(a)–8(c). Conversely, sanitization measures that increase ϵ reduce the number of infected individuals, as depicted in Figure 8(d). This finding suggests that eliminating the virus from contaminated environments can significantly limit the number of infections. Furthermore, a susceptible individual interacts with a contaminated environment at a transmission rate denoted by β_1. Figure 8(e) demonstrates that as β_1 increases, the infection levels rise.

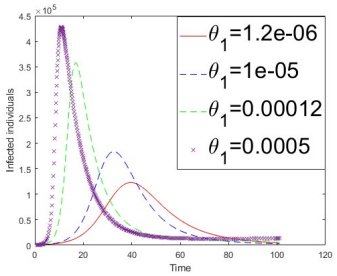

(a) Effect of θ_1 on I

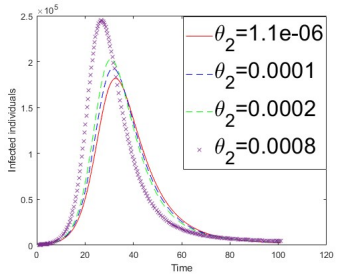

(b) Effect of θ_2 on I

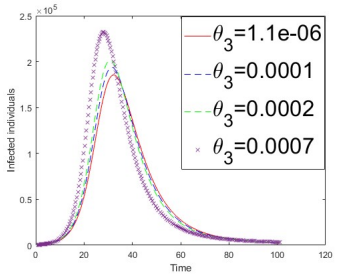

(c) Effect of θ_3 on I

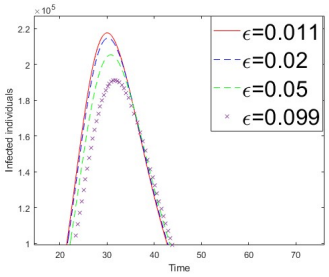

(d) Effect of ϵ on I

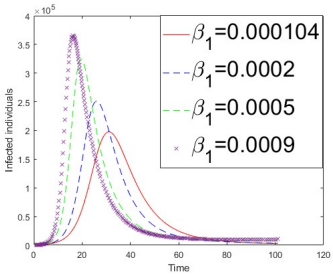

(e) Effect of β_1 on I

Figure 8: The effects of varying $\theta_1, \theta_2, \theta_3, \beta_1, \epsilon$ on the infected population I.

5 Optimal control

This section introduces an optimal control framework designed to determine the most effective control parameters. We consider the dynamical system $z'(t) = f(z(t))$ with the initial condition $z(0) = z_0$, where $z_0 \in \mathbb{R}^n$, $f : \mathbb{R}^n \to \mathbb{R}^n$, and $z : [0, \infty) \to \mathbb{R}^n$. To incorporate control interventions, we define control variable u_i, where $i \in \mathbb{N}$, leading to the controlled system,

$$z'(t) = f(z(t), u(t)), \quad z(0) = z_0,$$

with the control function $u : [0, \infty) \to A \subset \mathbb{R}^n$. The set of admissible controls is given by

$$X^* = \{u(t) \in L'(t_0, t_f) \, : \, u(t) \in A\}.$$

The primary objective is to determine the optimal control variables u_i that minimize the secondary transmission rate while also ensuring the associated implementation costs remain as low as possible over the time interval $t_0 \leq t \leq t_f$ [25]. We consider the following control variables:

1. $u_1 \equiv$ control of infections through nonpharmaceutical interventions such as face masks, hand sanitisers, etc., promoted by awareness campaigns.

2. $u_2 \equiv$ control of infections by reducing indirect transmission.

3. $u_3 \equiv$ control to enhance the uptake of the second vaccination dose.

4. $u_4 \equiv$ control to reduce virus release into the environment by encouraging infected individuals to take precautions, such as maintaining safe distances, covering coughs and sneezes with disposable tissues or clothing, and washing hands after coughing or sneezing.

5. $u_5 \equiv$ control for disinfecting contaminated environments.

To minimize both the total number of infectious cases and the corresponding implementation costs, we define the following objective function:

$$\begin{aligned} &J\left(u_1, u_2, u_3, u_4, u_5\right) \\ &= \min \int_{t_0}^{t_f} \left(Q + D_1 \frac{u_1^2}{2} + D_2 \frac{u_2^2}{2} + D_3 \frac{u_3^2}{2} + D_4 \frac{u_4^2}{2} + D_5 \frac{u_5^2}{2} \right) dt. \end{aligned} \tag{8}$$

where $Q = C_1 E + C_2 I_a + C_3 I + C_4 I_0 + C_5 U$, subject to constraints:

$$\begin{cases} \frac{dS}{dt} & = \Lambda - \frac{(1-u_1)\beta(\eta_1 I + I_a + \eta_2 I_0)S}{N} - (1-u_1-u_2)\beta_1 US - \nu_1 S + \omega_1 V_1 \\ & \quad + \chi R - \mu S, \\ \frac{dE}{dt} & = \frac{(1-u_1)\beta(\eta_1 I + I_a + \eta_2 I_0)(S+\theta V_1)}{N} + (1-u_1-u_2)\beta_1 US - \sigma E - \mu E, \\ \frac{dI_a}{dt} & = \psi\sigma E - \gamma_1 I_a - \mu I_a, \\ \frac{dI}{dt} & = (1-\psi-\phi)\,\sigma E - \gamma_2 I - \delta_1 I - \mu I, \\ \frac{dI_0}{dt} & = \phi\sigma E - \gamma_3 I_0 - \delta_2 I_0 - \mu I_0, \\ \frac{dV_1}{dt} & = \nu_1 S - (\nu_2 + \tau_1 u_3)V_1 - \omega_1 V_1 - \frac{(1-u_1)\theta\beta(\eta_1 I + I_a + \eta_2 I_0)V_1}{N} - \mu V_1, \\ \frac{dV_2}{dt} & = (\nu_2 + \tau_1 u_3)V_1 - \gamma_4 V_2 - \mu V_2, \\ \frac{dR}{dt} & = \gamma_2 I + \gamma_1 I_a + \gamma_3 I_0 + \gamma_4 V_2 - \chi R - \mu R, \\ \frac{dU}{dt} & = (1-u_4)\theta_2 I + (1-u_4)\theta_1 I_a + (1-u_4)\theta_3 I_0 - (\epsilon + \tau_2 u_5)U. \end{cases} \tag{9}$$

We begin by assuming the following initial conditions:

$$S(0) > 0, \quad E(0) \geq 0, \quad I_a(0) \geq 0, \quad I(0) \geq 0, \quad I_0(0) \geq 0, \quad V_1(0) \geq 0,$$

$$V_2(0) \geq 0, \quad R(0) \geq 0, \quad U(0) \geq 0.$$

In the optimization framework, the constants C_1, C_2, C_3, C_4, and C_5 act as weighting coefficients corresponding to the exposed individuals, the various infected groups (I_a, I, I_0), and the environmental viral concentration.

The time-dependent control parameters u_1, u_2, u_3, u_4, and u_5 are associated with the quadratic cost terms $D_1 u_1^2, D_2 u_2^2, D_3 u_3^2, D_4 u_4^2$, and $D_5 u_5^2$, respectively. These squared expressions represent the severity or magnitude of each control effort.

The existence of an optimal solution to the control problem is ensured by the conditions set forth in the Filippov–Cesari theorem [2]. The Hessian matrix of the cost functional is given by

$$\mathbf{D} = \mathrm{diag}(D_1, D_2, D_3, D_4, D_5),$$

which is positive definite everywhere. Therefore, the objective functional

$$J(u_1, u_2, u_3, u_4, u_5)$$

is strictly convex. As a result, there exists a minimum value

$$D = \min\{D_1, D_2, D_3, D_4, D_5\} > 0$$

that guarantees convexity in the integrand of the objective functional

$$\begin{aligned}&C_1E + C_2I_a + C_3I + C_4I_0 + C_5U + D_1\frac{u_1^2}{2} + D_2\frac{u_2^2}{2} + D_3\frac{u_3^2}{2} + D_4\frac{u_4^2}{2} + D_5\frac{u_5^2}{2}\\ &\geq D\left(u_1^2 + u_2^2 + u_3^2 + u_4^2 + u_5^2\right),\end{aligned}$$

This inequality is satisfied whenever $E + I_a + I + I_0 + U \geq 0$. Pontryagin's maximum principle is applied with respect to the defined state variables

$$S = S^*, \quad E = E^*, \quad I_a = I_a^*, \quad I = I^*, \quad I_0 = I_0^*, \quad V_1 = V_1^*,$$

$$V_2 = V_2^*, R = R^*, U = U^*.$$

We obtain the Hamiltonian function:

$$\begin{aligned}H =& C_1E^* + C_2I_a^* + C_3I^* + C_4I_0^* + C_5U^* + D_1\frac{u_1^2}{2} + D_2\frac{u_2^2}{2} + D_3\frac{u_3^2}{2}\\ &+ D_4\frac{u_4^2}{2} + D_5\frac{u_5^2}{2} + \lambda_1\frac{dS}{dt} + \lambda_2\frac{dE}{dt} + \lambda_3\frac{dI_a}{dt} + \lambda_4\frac{dI}{dt} + \lambda_5\frac{dI_0}{dt}\\ &+ \lambda_6\frac{dV_1}{dt} + \lambda_7\frac{dV_2}{dt} + \lambda_8\frac{dR}{dt} + \lambda_9\frac{dU}{dt}.\end{aligned}$$

The adjoint functions $\lambda_i, i = 1, 2, \ldots, 9$, obey the following equations:

$$\begin{aligned}\frac{d\lambda_1}{dt} &= -\frac{\partial H}{\partial S}\\ &= -(\lambda_6 - \lambda_2)\frac{(1-u_1)\theta\beta V_1(I_a + \eta_1 I + \eta_2 I_0)}{N^2} - (\lambda_6 - \lambda_1)\nu_1 + \mu\lambda_1\\ &\quad - (\lambda_2 - \lambda_1)\left(U(1-u_1-u_2)\beta_1 + \frac{(1-u_1)\beta(I_a + \eta_1 I + \eta_2 I_0)}{N}\right)\\ &\quad + (\lambda_2 - \lambda_1)\left(\frac{(1-u_1)\beta S(I_a + \eta_1 I + \eta_2 I_0)}{N^2}\right),\\ \frac{d\lambda_2}{dt} &= -\frac{\partial H}{\partial E}\\ &= -(\lambda_1 - \lambda_2)\frac{(1-u_1)\beta S(I_a + \eta_1 I + \eta_2 I_0)}{N^2}\\ &\quad - (\lambda_6 - \lambda_2)\frac{(1-u_1)\theta\beta V_1(I_a + \eta_1 I + \eta_2 I_0)}{N^2}\\ &\quad - \lambda_5\sigma\phi - \lambda_3\sigma\psi - \lambda_4\sigma(1-\phi-\psi) - C_1 + \lambda_2(\mu+\sigma),\\ \frac{d\lambda_3}{dt} &= -\frac{\partial H}{\partial I_a}\\ &= -\frac{(\lambda_2 - \lambda_1)((1-u_1)\beta S(N - \eta_1 I - \eta_2 I_0))}{N^2}\end{aligned}$$

$$
\begin{aligned}
&- \frac{(\lambda_2-\lambda_6)((1-u_1)\theta\beta V_1(N-\eta_1 I-\eta_2 I_0))}{N^2}\\
&- \gamma_1\lambda_8-(1-u_4)\theta_1\lambda_9+\lambda_3(\gamma_1+\mu)-C_2,\\
\frac{d\lambda_4}{dt} &= -\frac{\partial H}{\partial I}\\
&= -\frac{(\lambda_2-\lambda_1)((1-u_1)\beta S(\eta_1 N-I_a-\eta_1 I-\eta_2 I_0))}{N^2}\\
&- \frac{(\lambda_2-\lambda_6)((1-u_1)\theta\beta V_1(\eta_1 N-I_a-\eta_1 I-\eta_2 I_0))}{N^2}\\
&- \gamma_2\lambda_8-(1-u_4)\theta_2\lambda_9+\lambda_4(\gamma_2+\delta_1+\mu)-C_3,\\
\frac{d\lambda_5}{dt} &= -\frac{\partial H}{\partial I_0}\\
&= -\frac{(\lambda_2-\lambda_1)((1-u_1)\beta S(\eta_2 N-I_a-\eta_1 I-\eta_2 I_0))}{N^2}\\
&- \frac{(\lambda_2-\lambda_6)((1-u_1)\theta\beta V_1(\eta_2 N-I_a-\eta_1 I-\eta_2 I_0))}{N^2}\\
&- \gamma_3\lambda_8-(1-u_4)\theta_3\lambda_9+\lambda_5(\gamma_3+\delta_2+\mu)-C_4,\\
\frac{d\lambda_6}{dt} &= -\frac{\partial H}{\partial V_1}\\
&= \lambda_6\mu-(\lambda_7-\lambda_6)(\nu_2+u_3\tau_1)-(\lambda_1-\lambda_6)\omega_1\\
&- (\lambda_1-\lambda_2)\frac{(1-u_1)\beta S(I_a+\eta_1 I+\eta_2 I_0)}{N^2}\\
&- (\lambda_2-\lambda_6)\frac{(1-u_1)\theta\beta(N-V_1)(I_a+\eta_1 I+\eta_2 I_0)}{N^2},\\
\frac{d\lambda_7}{dt} &= -\frac{\partial H}{\partial V_2}\\
&= -\frac{(1-u_1)\beta(I_a+\eta_1 I+\eta_2 I_0)(S(\lambda_1-\lambda_2)+V_1\theta(\lambda_6-\lambda_2))}{N^2}\\
&- \gamma_4(\lambda_8-\lambda_7)+\lambda_7\mu,\\
\frac{d\lambda_8}{dt} &= -\frac{\partial H}{\partial R}\\
&= -\frac{1}{N^2}((\lambda_1-\lambda_2)(1-u_1)\beta S(I_a+\eta_1 I+\eta_2 I_0))\\
&- \frac{1}{N^2}((\lambda_6-\lambda_2)(1-u_1)\theta\beta V_1(I_a+\eta_1 I+\eta_2 I_0))-\lambda_1\chi+\lambda_8(\mu+\chi),\\
\frac{d\lambda_9}{dt} &= -\frac{\partial H}{\partial U}\\
&= -C_5+(1-u_1-u_2)\beta_1 S(\lambda_1-\lambda_2)+\lambda_9(\epsilon+u_5\tau_2).
\end{aligned}
\tag{10}
$$

Imposing the terminal condition $\lambda_i(t_f)=0$ for $i=1,2,\ldots,9$, and using the requirement that $\frac{\partial H}{\partial u_i}=0$ for all u_i, the corresponding optimal control law is given by

$$u_1^* = \min\left\{ \max\left(0, \frac{\beta_1(\lambda_2-\lambda_1)N^*S^*U^* + \beta(I_a^* + \eta_1 I^* + \eta_2 I_0^*)(S^*(\lambda_2-\lambda_1) + \theta V_1^*(\lambda_2-\lambda_6))}{D_1 N^*}\right), u_{1\max}\right\},$$

$$\begin{aligned}
u_2^* &= \min\left\{ \max\left(0, \frac{\beta_1(-\lambda_1+\lambda_2)S^*U^*}{D_2}\right), u_{2\max}\right\},\\
u_3^* &= \min\left\{ \max\left(0, \frac{(\lambda_6-\lambda_7)\tau_1 V_1^*}{D_3}\right), u_{3\max}\right\},\\
u_4^* &= \min\left\{ \max\left(0, \frac{(\theta_1 I_a^* + \theta_2 I^* + \theta_3 I_0^*)\lambda_9}{D_4}\right), u_{4\max}\right\},\\
u_5^* &= \min\left\{ \max\left(0, \frac{\lambda_9\tau_2 U^*}{D_5}\right), u_{5\max}\right\}.
\end{aligned}$$

5.1 Numerical solution of the model under optimal control

In this subsection, we conduct numerical experiments for the optimal control model to investigate how different time-dependent control strategies affect the transmission dynamics of the disease.

The simulations use the parameter set given in Table 2; several of these parameters are obtained by fitting the model to COVID-19 data reported for India. For the computations, India's total population is taken to be approximately 1.40 billion, which serves as the reference population size. To compute the optimal control, we employ the forward-backward sweep algorithm described in [2].

The trajectories displayed in Figures 9(a)–9(e) show, separately, the influence of each control variable u_i $(i = 1, 2, 3, 4, 5)$ on the state variables E, I_a, I, I_0 and U. In these plots, the solid curves represent the scenario without control, while the dotted curves indicate the system with the control strategy in place. The implementation of control measures significantly reduces both the infected population and the environmental viral load.

Figure 10 presents the optimal time profiles of the controls u_1, u_2, u_3, u_4 and u_5 and their impact on the spread of COVID-19 in the human population and the environment. In Figure 10(a), u_1 reaches its maximum value during the initial days and remains at this level until approximately $t = 90$ days. A similar pattern is observed in Figure 10(b) for u_2, which also attains an early peak and maintains this maximum level up to $t = 90$ days. In contrast, Figure 10(c) shows that u_3 reaches its highest value between 30 and 60 days and then gradually decreases until $t = 100$ days. Figure 10(d) indicates that u_4 peaks in the interval 0–50 days, followed by a

slow decline up to $t = 100$ days. Finally, Figure 10(e) reveals that u_5 also reaches its maximum between 0 and 70 days and then steadily diminishes until $t = 100$ days.

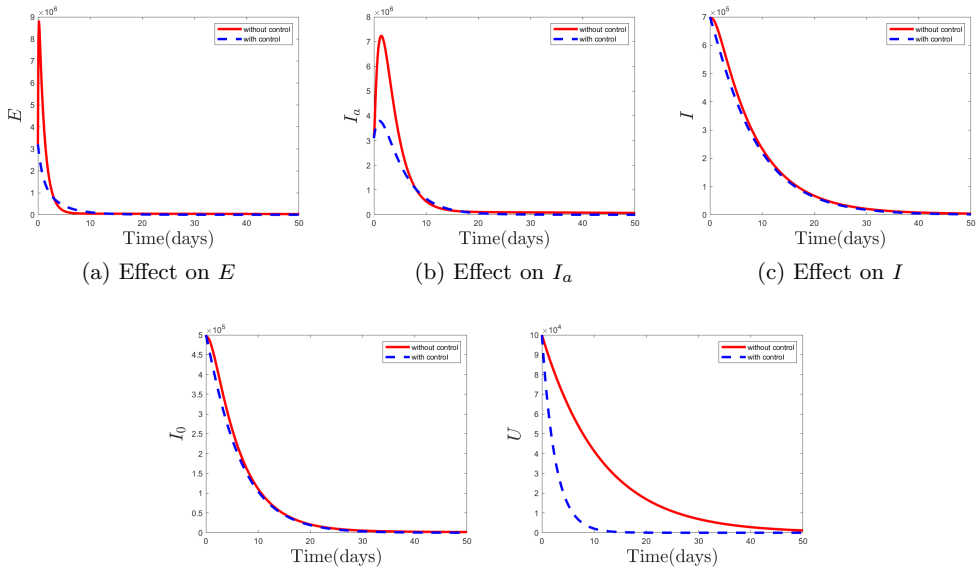

(a) Effect on E (b) Effect on I_a (c) Effect on I

(d) Effect on I_0 (e) Effect on U

Figure 9: Effect of control measures: u_1, u_2, u_3, u_4, u_5

Table 4: Scenarios and their combination strategy

Scenario	**Strategies**
A	S-1. $(u_1 \neq 0, u_2 = 0, u_3 = 0, u_4 = 0, u_5 = 0)$
	S-2. $(u_1 = 0, u_2 \neq 0, u_3 = 0, u_4 = 0, u_5 = 0)$
	S-3. $(u_1 = 0, u_2 = 0, u_3 \neq 0, u_4 = 0, u_5 = 0)$
B	S-4. $(u_1 \neq 0, u_2 \neq 0, u_3 \neq 0, u_4 = 0, u_5 = 0)$
C	S-5. $(u_1 \neq 0, u_2 \neq 0, u_3 \neq 0, u_4 \neq 0, u_5 \neq 0)$

To achieve efficient resource allocation while reducing the economic burden associated with controlling the transmission of COVID-19, we implement selective intervention strategies based on different combinations of time-dependent control variables instead of employing all five controls simultaneously. This framework enables a comparative assessment of multiple intervention schemes (see Table 4) and facilitates the evaluation of their relative efficiency, implementation costs, and epidemiological outcomes.

Three intervention scenarios, namely Scenarios A, B, and C, are considered according to the control strategies summarized in Table 4 and illustrated in Figures 11(a)–11(e). In Scenario A,

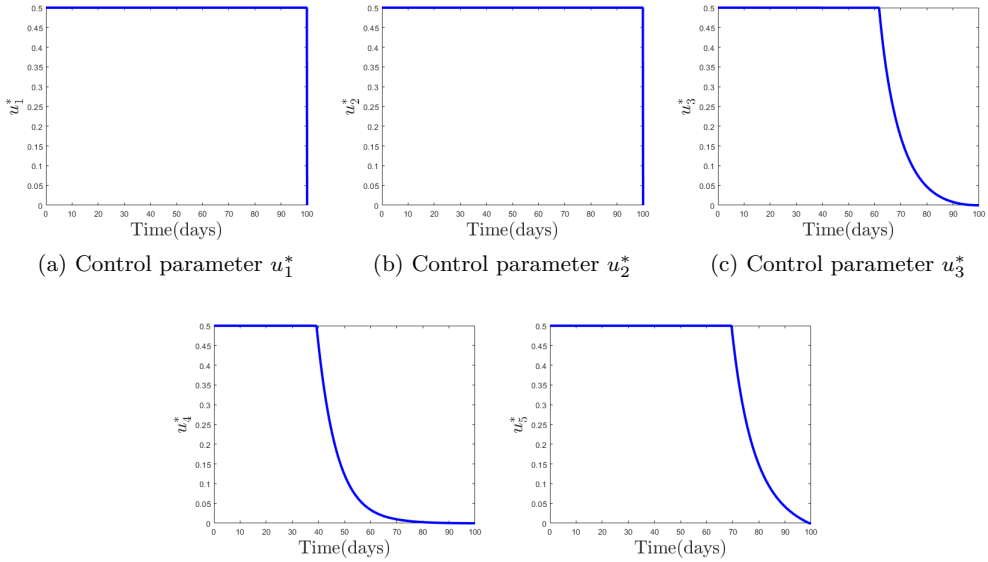

(a) Control parameter u_1^* (b) Control parameter u_2^* (c) Control parameter u_3^*

(d) Control parameter u_4^* (e) Control parameter u_5^*

Figure 10: Control profiles: u_1, u_2, u_3, u_4 and u_5

the control measures u_1, u_2, and u_3 are evaluated individually, whereas u_4 and u_5 are excluded (Figures 11(a)–11(c)). Scenario B examines the combined implementation of strategies S-1, S-2, and S-3, with the corresponding simulation results presented in Figure 11(d). Scenario C represents the comprehensive intervention strategy in which all five control variables, u_1, u_2, u_3, u_4, and u_5, are applied simultaneously, as illustrated in Figure 11(e).

The simulation results indicate that intervention measures directed toward the infectious compartments, represented by u_1, u_2, and u_3, contribute more substantially to suppressing disease transmission than the environmental control measures u_4 and u_5. Furthermore, the simultaneous implementation of controls across all infectious classes (Figure 11(d)) produces a more pronounced reduction in disease prevalence than strategies in which these controls are applied separately (Figures 11(a)–11(c)). Among the three investigated scenarios, Scenario C consistently provides the greatest reduction in disease transmission, demonstrating that the integrated application of all available control measures is the most effective strategy for mitigating the spread of COVID-19 (Figure 11(e)).

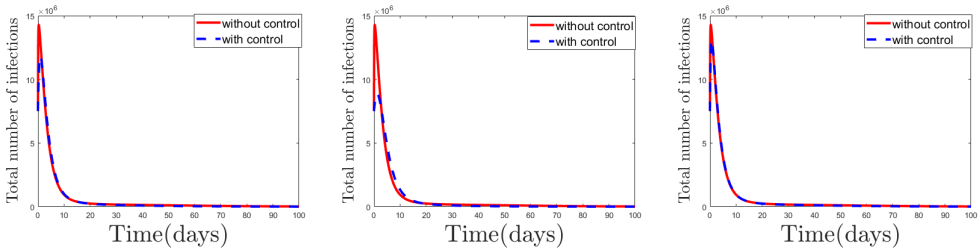

(a) S-1: control u_1 only (b) S-2: control u_2 only (c) S-3: control u_3 only

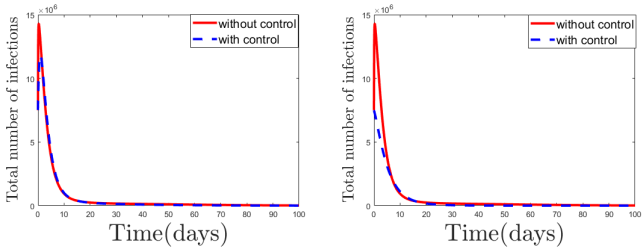

(d) S-4: u_1, u_2 and u_3 only (e) S-5: u_1, u_2, u_3, u_4 and u_5

Figure 11: Effect of control u_1, u_2, u_3, u_4 and u_5 on total number of infections

6 Discussion and conclusion

In the present study, we developed a new mathematical model to study the transmission dynamics of COVID-19. The model focuses on the Omicron variant and incorporates individuals who have received the first and second doses of the vaccine. By integrating environmental contamination into the model, we introduce an additional layer of complexity that better represents real-world conditions, particularly in areas heavily impacted by Omicron.

The model was analyzed using dynamical systems approach, emphasizing solution positivity, boundedness, and the biological relevance of the control reproduction number derived from the next-generation matrix. Stability analysis was conducted for both the disease-free and endemic equilibria.

The numerical simulations for the proposed model, detailed in Section 4, used COVID-19 data from India, collected between December 30, 2021, and April 30, 2022, from Johns Hopkins University [16]. Figure 6(c) illustrates that vaccination plays a crucial role in shaping the dynamics of the disease. A normalized forward sensitivity analysis is conducted on the control reproduction number R_c with respect to model parameters, revealing that the transmission rate is the most significant factor. PRCC sensitivity indices are computed using the LHS technique, taking $I(t)$ as a response function with respect to model parameters. PRCC sensitivity indices

show a robust negative correlation between the infected population I and ψ (as seen in Figure 3(b)).

The analysis further demonstrated that the first dose of the vaccine provides incomplete protection, making it essential to maintain a low waning rate of immunity (ω_1) to minimize infection levels (Figure 6(d)). As ω_1 increases, the infection peak increases, indicating a greater risk of infection due to the return of vaccinated individuals to the susceptible class, which can be mitigated through the administration of a second dose. Figure 7(a) illustrates the impact of first-dose vaccine efficacy $(1-\theta)$, highlighting the need to optimize efficacy through booster doses, public health measures, and timely vaccinations to effectively manage the pandemic.

Additionally, we examined the impact of waning immunity $(1/\chi)$ on infection levels, which is critical for understanding reinfection dynamics (Figure 7(b)). Environmental contamination effects were also studied (Figure 8), with findings showing a decline in infection peaks as viral removal efforts (ϵ) increased (Figure 8(d)). This underscores the importance of safety measures, such as maintaining physical distance, covering coughs and sneezes, and practicing good hygiene to reduce community transmission.

We extended the model to incorporate an optimal control problem, examining nonpharmaceutical interventions such as face masks and hand sanitisers, reducing indirect transmission, administering the second vaccine dose, and disinfecting contaminated environments. Using Pontryagin's Maximum Principle, we established the conditions for optimal control and employed the forward-backward sweep method to assess the impact of these strategies. Numerical simulations, as shown in Figure 11(e), demonstrate that Scenario C, which combines all control variables, is the most effective in mitigating disease spread while minimizing the associated intervention costs. Overall, the results suggest that five distinct control measures should be dynamically adjusted to effectively reduce both infections and associated costs, with the second vaccine dose emerging as the most effective strategy for curbing widespread transmission.

Future research could explore extending the proposed model into a fractional-order model, as studies have shown that fractional derivatives possess additional characteristics not present in integer-order derivatives [17, 33]. Such an extension may provide a more comprehensive understanding of COVID-19 dynamics.

Funding

This study was conducted without financial support from any particular funding organization.

Conflicts of Interest

No potential conflicts of interest are associated with this research.

Data availability

All the data used in this article can be accessed freely through the website https://data.humdata.org/dataset/novel-coronavirus-2019-ncov-cases#data-resources-0.

Author contributions

Amit Singh Thakur: Writing – original draft, Visualization, Validation, Methodology, Investigation, Formal analysis, Conceptualization. Govind Prasad Sahu: Writing – review & editing, Supervision. Chhatrpal Singh Sikarwar: Review & editing. Harkaran Singh: Review & editing.

References

[1] Asamoah, J.K.K., Owusu, M.A., Jin, Z., Oduro, F.T., Abidemi, A. and Gyasi, E.O. *Global stability and cost-effectiveness analysis of COVID-19 considering the impact of the environment: Using data from Ghana*, Chaos Solitons Fractals 140 (2020), 110103.

[2] Atangana, A. and Iġret, A.S. *Mathematical model of COVID-19 spread in Turkey and South Africa: Theory, methods, and applications*, Adv. Differ. Equations 2020(1) (2020), 1–89.

[3] Bagal, D.K., Rath, A., Barua, A. and Patnaik, D. *Estimating the parameters of susceptible-infected-recovered model of COVID-19 cases in India during lockdown periods*, Chaos Solitons Fractals 140 (2020), 110154.

[4] Bai, X. and Ma, S. *Stochastic dynamical behavior of COVID-19 model based on secondary vaccination*, Math. Biosci. Eng. 20(2) (2023), 2980–2997.

[5] Bajiya, V.P., Bugalia, S., Tripathi, J.P. and Martcheva, M. *Deciphering the transmission dynamics of COVID-19 in India: Optimal control and cost effective analysis*, J. Biol. Dyn. 16(1) (2022), 665–712.

[6] Bandekar, S.R., Das, T., Srivastav, A.K., Yadav, A., Kumar, A., Srivastava, P.K. and Ghosh, M. *Modeling and prediction of the third wave of COVID-19 spread in India*, Comput. Math. Biophys. 10(1) (2022), 231–248.

[7] Birkhoff, G. and Rota, G. *Ordinary differential equations*, Wiley, United Kingdom, 1978.

[8] Castillo-Chavez, C. and Song, B. *Dynamical models of tuberculosis and their applications*, Math. Biosci. Eng. 1(2) (2004), 361–404.

[9] Chavda, V.P., Bezbaruah, R., Deka, K., Nongrang, L. and Kalita, T. *The Delta and Omicron variants of SARS-CoV-2: What we know so far*, Vaccines 10(11) (2022), 1926.

[10] Davies, N.G., Abbott, S., Barnard, R.C., Jarvis, C.I., Kucharski, A.J., Munday, J.D., Pearson, C.A., Russell, T.W., Tully, D.C., Washburne, A.D. and Wenseleers, T. *Estimated transmissibility and impact of SARS-CoV-2 lineage B.1.1.7 in England*, Science 372(6538) (2021), eabg3055.

[11] Fisher, A., Xu, H., He, D. and Wang, X. *Effects of vaccination on mitigating COVID-19 outbreaks: A conceptual modeling approach*, Math. Biosci. Eng. 20(3) (2023), 4816–4837.

[12] Foy, B.H., Wahl, B., Mehta, K., Shet, A., Menon, G.I. and Britto, C. *Comparing COVID-19 vaccine allocation strategies in India: A mathematical modelling study*, Int. J. Infect. Dis. 103 (2021), 431–438.

[13] Ghosh, B. *Fractional order modeling of ecological and epidemiological systems: Ambiguities and challenges*, J. Anal. 33(1) (2025), 341–366.

[14] Guo, Y. and Li, T. *Modeling the competitive transmission of the Omicron strain and Delta strain of COVID-19*, J. Math. Anal. Appl. 526(2) (2023), 127283.

[15] He, X., Chen, H., Zhu, X. and Gao, W. *Non-pharmaceutical interventions in containing COVID-19 pandemic after the roll-out of coronavirus vaccines: A systematic review*, BMC Public Health 24(1) (2024), 1–11.

[16] Humanitarian Data Exchange, *Novel coronavirus 2019 (COVID-19) cases*, https://data.humdata.org/dataset/novel-coronavirus-2019-ncov-cases#data-resources-0 (accessed June 2023).

[17] Joshi, H., Jha, B.K. and Yavuz, M. *Modelling and analysis of fractional-order vaccination model for control of COVID-19 outbreak using real data*, Math. Biosci. Eng. 20(1) (2023), 213–240.

[18] Karim, S.S.A. and Karim, Q.A. *Omicron SARS-CoV-2 variant: A new chapter in the COVID-19 pandemic*, Lancet 398(10317) (2021), 2126–2128.

[19] Kar, T.K. and Ghosh, B. *Sustainability and optimal control of an exploited prey–predator system through provision of alternative food to predator*, Biosystems 109(2) (2012), 220–232.

[20] Khan, M.A. and Atangana, A. *Mathematical modeling and analysis of COVID-19: A study of new variant Omicron*, Physica A 599 (2022), 127452.

[21] Kreabkhontho, P., Teparos, W. and Theparod, T. *Potential for eliminating COVID-19 in Thailand through third-dose vaccination: A modeling approach*, Math. Biosci. Eng. 21(8) (2024), 6807–6828.

[22] Li, T. and Guo, Y. *Modeling and optimal control of mutated COVID-19 (Delta strain) with imperfect vaccination*, Chaos Solitons Fractals 156 (2022), 111825.

[23] Li, X.N., Huang, Y., Wang, W., Jing, Q.L., Zhang, C.H., Qin, P.Z., Guan, W.J., Gan, L., Li, Y.L., Liu, W.H. and Dong, H. *Effectiveness of inactivated SARS-CoV-2 vaccines against the Delta variant infection in Guangzhou: A test-negative case–control real-world study*, Emerg. Microbes Infect. 10(1) (2021), 1751–1759.

[24] Mahajan, A., Sivadas, N.A. and Solanki, R. *An epidemic model SIPHERD and its application for prediction of the spread of COVID-19 infection in India*, Chaos Solitons Fractals 140 (2020), 110156.

[25] Martcheva, M. *An introduction to mathematical epidemiology*, Springer, United States, 2015.

[26] Mohankumar, N., Rajagopal, L. and Nieto, J.J. *Optimal control for co-infection with COVID-19-associated pulmonary aspergillosis in ICU patients with environmental contamination*, Math. Biosci. Eng. 20(6) (2023), 9861–9875.

[27] Negi, S.S., Rana, P.S., Sharma, N. and Khatri, M.S. *A novel SEIAHR compartment model for accessing the impact of vaccination, intervention policies, and quarantine on the COVID-19 pandemic: A case study of most affected countries Brazil, India, Italy, and USA*, Comput. Appl. Math. 41(7) (2022), 305.

[28] Omede, B., Odionyenma, U., Ibrahim, A. and Bolaji, B. *Third wave of COVID-19: Mathematical model with optimal control strategy for reducing the disease burden in Nigeria*, Int. J. Dyn. Control 11(1) (2023), 411–427.

[29] Omorogie, E.O., Owolabi, K.M. and Olabode, B.T. *A non-linear deterministic mathematical model for investigating the population dynamics of COVID-19 in the presence of vaccination*, Healthc. Anal. 5 (2024), 1–13.

[30] Özüdoğru, O., Bahçe, Y.G. and Acer, Ö. *SARS-CoV-2 reinfection rate is higher in the Omicron variant than in the Alpha and Delta variants*, Ir. J. Med. Sci. 192(2) (2023), 751–756.

[31] Ou, J., Lan, W., Wu, X., Zhao, T., Duan, B., Yang, P., Ren, Y., Quan, L., Zhao, W., Seto, D. and Chodosh, J. *Tracking SARS-CoV-2 Omicron diverse spike gene mutations identifies multiple inter-variant recombination events*, Signal Transduct. Target. Ther. 7(1) (2022), 138.

[32] Pai, C., Bhaskar, A. and Rawoot, V. *Investigating the dynamics of COVID-19 pandemic in India under lockdown*, Chaos Solitons Fractals 138 (2020), 109988.

[33] Panwar, V.S., Uduman, P.S. and Gómez-Aguilar, J. *Mathematical modeling of coronavirus disease COVID-19 dynamics using CF and ABC non-singular fractional derivatives*, Chaos Solitons Fractals 145 (2021), 110757.

[34] Prakash, D.B., Chhetri, B., Vamsi, D.K.K., Balasubramanian, S. and Sanjeevi, C.B. *Low temperatures or high isolation delay increases the average COVID-19 infections in India: A mathematical modeling approach*, Comput. Math. Biophys. 9 (2021), 146–174.

[35] Perra, N. *Non-pharmaceutical interventions during the COVID-19 pandemic: A review*, Phys. Rep. 913 (2021), 1–52.

[36] Rana, R., Kant, R., Huirem, R.S., Bohra, D. and Ganguly, N.K. *Omicron variant: Current insights and future directions*, Microbiol. Res. 265 (2022), 127204.

[37] Sahu, G.P. and Thakur, A.S. *Mathematical modeling of COVID-19 spread with media coverage and optimal control analysis*, Iran. J. Numer. Anal. Optim. 15(3) (2025), 952–992.

[38] Sahu, G.P. and Thakur, A.S. *Analyzing the role of media, environment, and treatment limits in epidemic spread: A mathematical and optimal control approach*, Netw. Model. Anal. Health Informatics Bioinform. 14(1) (2025), 87.

[39] Sardar, T., Nadim, S.K.S., Rana, S. and Chattopadhyay, J. *Assessment of lockdown effect in some states and overall India: A predictive mathematical study on COVID-19 outbreak*, Chaos Solitons Fractals 139 (2020), 1–10.

[40] Sarkar, K., Mondal, J. and Khajanchi, S. *How do the contaminated environment influence the transmission dynamics of COVID-19 pandemic?*, Eur. Phys. J. Spec. Top. 231(18–20) (2022), 3697–3716.

[41] Senapati, A., Rana, S., Das, T. and Chattopadhyay, J. *Impact of intervention on the spread of COVID-19 in India: A model based study*, J. Theor. Biol. 523 (2021), 110711.

[42] Selvamuthu, D., Khichar, D., Kalita, P. and Jain, V. *Estimation of mortality rate of COVID-19 in India using SEIRD model*, Opsearch 60(1) (2023), 539–553.

[43] Shringi, S., Sharma, H., Rathie, P.N., Bansal, J.C. and Nagar, A. *Modified SIRD model for COVID-19 spread prediction for northern and southern states of India*, Chaos Solitons Fractals 148 (2021), 111039.

[44] Shervani, Z., Bhardwaj, D., Hasan, S., Umair, Y., Qazi, M.P., Ibbrahim, A., Vuyyuru, V.P.S.R., Siddiquie, A., Sherwani, A.A., Khan, A.A., Fatma, K., Siddiqui, S., Jamal, N. and Khan, S. *The Omicron wave in India, Mumbai, and Delhi: Prevalence and pathogenicity*, Eur. J. Med. Health Sci. 4(3) (2022), 123–130.

[45] Sheng, Y., Cui, J.-A. and Guo, S. *The modeling and analysis of the COVID-19 pandemic with vaccination and isolation: A case study of Italy*, Math. Biosci. Eng. 20(3) (2023), 5966–5992.

[46] Saha, S., Samanta, G. and Nieto, J.J. *Impact of optimal vaccination and social distancing on COVID-19 pandemic*, Math. Comput. Simul. 200 (2022), 285–314.

[47] Shan, S., Luo, S., Yang, Z., Hong, J., Su, Y., Ding, F., Fu, L., Li, C., Chen, P., Ma, J. and Shi, X. *Deep learning guided optimization of human antibody against SARS-CoV-2 variants with broad neutralization*, Proc. Nat. Acad. Sci. 119(11) (2022), e2122954119.

[48] Singh, K., Verma, A. and Lakshminarayan, M. *India's efforts to achieve 1.5 billion COVID-19 vaccinations: A narrative review*, Osong Public Health Res. Perspect. 13(5) (2022), 316.

[49] Sooknanan, J. and Comissiong, D. *Trending on social media: Integrating social media into infectious disease dynamics*, Bull. Math. Biol. 82(7) (2020), 86.

[50] Sooknanan, J. and Mays, N. *Harnessing social media in the modelling of pandemics: Challenges and opportunities*, Bull. Math. Biol. 83(5) (2021), 57.

[51] Thakur, A.S. and Sahu, G.P. *Modeling the COVID-19 dynamics with Omicron variant, non-pharmaceutical interventions, and environmental contamination*, Differ. Equations Dyn. Syst. (2025), 1–25.

[52] Ullah, S. and Khan, M.A. *Modeling the impact of non-pharmaceutical interventions on the dynamics of novel coronavirus with optimal control analysis with a case study*, Chaos Solitons Fractals 139 (2020), 110075.

[53] Van den Driessche, P. and Watmough, J. *Reproduction numbers and subthreshold endemic equilibria for compartmental models of disease transmission*, Math. Biosci. 180(1–2) (2002), 29–48.

[54] Van Doremalen, N., Bushmaker, T., Morris, D.H., Holbrook, M.G., Gamble, A., Williamson, B.N., Tamin, A., Harcourt, J.L., Thornburg, N.J., Gerber, S.I. and Lloyd-Smith, J.O. *Aerosol and surface stability of SARS-CoV-2 as compared with SARS-CoV-1*, N. Engl. J. Med. 382(16) (2020), 1564–1567.

[55] Vivekanandhan, G., Zavareh, M.N., Natiq, H., Nazarimehr, F., Rajagopal, K. and Svetec, M. *Investigation of vaccination game approach in spreading COVID-19 epidemic model with considering the birth and death rates*, Chaos Solitons Fractals 163 (2022), 112565.

[56] Wang, X., Wang, H., Ramazi, P., Nah, K. and Lewis, M. *From policy to prediction: Forecasting COVID-19 dynamics under imperfect vaccination*, Bull. Math. Biol. 84(9) (2022), 90.

[57] World Health Organization, *Coronavirus disease (COVID-19)*, https://www.who.int/health-topics/coronavirus#tab=tab_1 (accessed July 2023).

[58] Yapışkan, D., Yurtoğlu, M., Avcı, D., İskender Eroğlu, B.B. and Bonyah, E. *A novel model for monkeypox disease: System analysis and optimal preventive strategies*, Iran. J. Sci. 47(5) (2023), 1665–1677.